Lung Cancer Classification using Reinforcement Learning-based Ensemble Learning

Shengping Luo*
College of Physics and Electronic Information, Nanchang Normal University
Nanchang 330000, Jiangxi, China

***Abstract*—Lung cancer is a significant health issue affecting millions of people worldwide annually. However, current manual detection methods used by physicians and radiologists to identify lung nodules are inefficient because of the diverse shapes and locations of the nodules in the lungs. New methods are needed to improve the accuracy and speed of detecting lung nodules. This is important because early detection of nodules can increase the likelihood of successful treatment and recovery. This paper introduces a new LLC-QE model that combines ensemble learning and reinforcement learning to classify lung cancer. Initially, the model undergoes pre-training through the utilization of the Artificial Bee Colony (ABC) algorithm. This approach aims to decrease the probability of the model getting stuck in a local optimum. Subsequently, a set of convolutional neural networks (CNNs) is used to simultaneously derive feature vectors from input images, which are subsequently combined for classification in downstream processes. The LIDC-IDRI dataset, predominantly composed of cases without cancer, was employed to train and evaluate the model. To mitigate the dataset imbalance, the training procedure using reinforcement learning is formulated as a series of interconnected decisions. During this process, the images are regarded as states; the network acts as the agent, and the agent is given a greater reward/punishment for accurately/incorrectly classifying the underrepresented class compared to the overrepresented class. The LLC-QE model achieves excellent results (F measure 89.8%; geometric mean 92.7%), outperforming other deep models. Identifying the optimal values for the reward function and determining the ideal number of CNN feature extractors in the ensemble are achieved through experiments conducted on the study dataset. Ablation studies that exclude ABC pre-training and reinforcement learning from the model confirm these components' independent positive incremental impact on the model's performance.**

***Keywords*—Lung cancer; ensemble learning; reinforcement learning; artificial bee colony; convolutional neural network**

I. Introduction

In recent years, the global mortality rate for lung cancer has risen significantly. This indicates that lung cancer has emerged as among the deadliest forms of cancer in recent decades [1]. However, over 50% of lung cancers can be treated successfully if detected early [2, 3]. Automatic cancer detection can significantly reduce the time required for diagnosis, leading to timely treatment. Sufficient forms of lung cancer are not visible to the naked eye, making automated diagnosis a valuable tool in reducing human error [4]. The computer-aided diagnosis (CAD) system can assist radiologists in rapidly and precisely detecting and diagnosing abnormalities. This can aid in identifying and diagnosing lung cancer at an earlier stage, resulting in more effective treatment options [5].

Computed tomography (CT) is a widely used method for detecting lung cancer, leading to an increase in CT images and putting pressure on radiologists [6]. To ease this burden, Computer-Aided Diagnosis (CAD) systems have been developed to aid in nodule detection [7, 8]. Detecting nodules is a complex task given their various sizes, shapes, and positions. Deep learning, particularly in CAD, has shown potential to enhance nodule detection. Examples include ZNET [9] using the U-Net architecture [10], Resnet utilizing a 3D CNN, and JianPeiCAD [11], which employs a multi-scale rule-based approach followed by a broad-channeled 3D CNN. While 3D CNNs capture CT scans' details, they come with longer training times and higher storage needs. The varying slice thickness in CT scans complicates 3D imaging, making 2D imaging more suitable in terms of training duration and resource use, making it a preferred method for nodule identification.

Imbalanced class distribution is a pressing issue in deep learning, especially in lung cancer classification, where the uneven spread between positive and negative cases hampers model accuracy [12]. To address this, data-level methods like over-sampling and under-sampling are employed. Over-sampling, such as Synthetic Minority Oversampling Technique (SMOTE) [13], creates synthetic examples for the minority class, while under-sampling techniques like NearMiss [14] reduce majority class instances. However, these can lead to overfitting or loss of vital data. Algorithm-level solutions amplify the minority class's influence using ensemble learning, cost-sensitive methods, and decision threshold adjustments. Cost-sensitive techniques assign different misclassification costs, ensemble methods utilize multiple classifiers, and threshold adjustments modify the classification threshold during tests. Some deep learning strategies focus on learning distinct features in unbalanced data or ensure balanced mini-batch training in convolutional networks. These approaches aim to improve classification precision in the face of imbalanced data [15].

In the past several years, deep reinforcement learning (DRL) [16] demonstrated successful applications in various areas, including computer games, robot control, and recommendation systems. DRL helps in removing noisy data and enhancing features, which ultimately boosts the performance of the classification system [17]. The classification process is a sequential decision-making task that requires the acquisition of an optimized policy. However, the

computational time required for the process is amplified due to the elaborate simulations conducted between agents and environments. Some researchers have utilized deep reinforcement learning to learn valuable data features and enhance the useful features of the classifier [18-21]. An ensemble pruning approach has also been developed, which selects the best sub-classifiers with the help of RL, which is effective for small data [22]. However, there has been a minimal investigation into using DPL in imbalanced classification, particularly in medical images. DPL is suitable for imbalanced classification as it rewards or penalizes the minority class more to attract more attention.

ABC [23] is utilized for optimization, inspired by the manner in which honeybees hunt for food. The algorithm imitates the way bees search for food sources by using three components: employed bees, onlooker bees, and scout bees. Bees in the workforce have the duty of finding food sources and communicating their whereabouts to other bees by performing a waggle dance. Onlooker bees then choose the most promising food sources based on the information they received from the employed bees. Scout bees search for new food sources when the current ones are depleted. ABC has proven effective in tackling multiple optimization problems [24], one of which is the initialization of neural network weights [12]. It has shown promising results in improving the performance of deep neural networks and reducing the effect of suboptimal solutions caused by parameter initialization [25]. In addition, the ABC algorithm is a straightforward approach that causes tuning only a few parameters and is simple to implement. As a result, it can be considered a dependable and effective substitute for backpropagation in the training of neural networks.

This paper presents a model called LLC-QE based on deep Q-learning and ensemble learning, combined with the ABC algorithm for weight initialization. Classification is considered a guessing game using a Markov decision process within an RL framework. The state of the environment is represented by a CT image of the patient, and the agent is a deep neural network comprising several parallel convolutional feature extractors. To start the game, the investigation revolves around employing the ABC algorithm in LLC-QE. This algorithm targets the discovery of weight initializations for CNNs and feed-forward networks within the backpropagation algorithm. The agent then decides whether the patient is healthy or ill, and the decision is rewarded with correct decisions receiving positive rewards and incorrect ones receiving negative rewards. In order to address the dataset imbalance, a greater absolute value of the reward is given to the minority class. The aim of the agent is to maximize its cumulative rewards throughout the sequential decision-making process, which involves classifying the samples with the highest possible accuracy. The performance of the LLC-QE model is evaluated on the widely used LIDC-IDRI dataset, and the results show its superiority over other approaches that rely on random weight initialization.

The article is structured in this manner: Section II gives a broad summary of various techniques employed in examining lung nodules. Section III delves deep into the methodology we suggest. Section IV outlines the dataset used for the research and showcases the experimental outcomes. Lastly, Section V wraps up the discussion and proposes potential avenues for further study.

II. Related Work

CAD is a popular technique for detecting pulmonary nodules in medical images [26]. Conventional methods usually require manually creating features, such as setting pixel thresholds, grouping voxels, and using morphological characteristics. However, these methods are often limited by their ability to detect nodules accurately and to distinguish them from false positives [27]. Tan et al. [28] created a CAD system based on CNN that uses a nodule segmentation technique to detect nodule clusters' central positions in the detection phase. The method integrates computed divergence features with nodule and vessel enhancement filters. In the classification stage, distinctive features that are invariant and defined on a gauge coordinate system are employed to distinguish genuine nodules from certain types of blood vessels that can result in inaccurate positive identifications. Another approach to CAD system development is to merge two or more existing CAD sub-systems to improve accuracy. Traverso and colleagues [29] developed a CAD system that operates through the web and cloud by merging two separate CAD sub-systems: the Channeler Ant Model and the Voxel-Based Neural Approach (VBNA). Both algorithms share a starting point, which involves utilizing a three-dimensional (3D) region-growing segmentation method to obtain the parenchymal volume while simultaneously eliminating the trachea and dividing the two lungs. The Channeler Ant Model utilizes an ant-colony optimization algorithm to identify nodule candidates, while the VBNA uses a multi-layer perceptron neural network to classify them.

In recent times, the field of computer vision has undergone a revolution with the emergence of deep learning, especially CNNs. CNNs have demonstrated remarkable performance in extracting pertinent features from images that can be employed for tasks, such as object detection and classification [30, 31]. This has led to significant advances in fields ranging from medical imaging to autonomous driving. One of the key advantages of CNNs is their ability to learn features in an end-to-end method with no hand-crafted features or feature engineering. This means that CNNs can learn to recognize complex patterns and features in images, such as edges, corners, and textures, by processing the raw pixel values directly. This has led to significant improvements in image classification accuracy on benchmark datasets, such as ImageNet, where CNNs have achieved human-level performance. Another important advantage of CNNs is their ability to generalize to new tasks and datasets. Transfer learning refers to a methodology that enables pre-trained CNNs to apply to new datasets or tasks. This can be done by fine-tuning the model on the new data or by employing the network as a fixed feature extractor. This has been effective for a wide range of tasks, from medical image analysis to natural language processing. There are several well-known frameworks for object detection that utilize CNNs, such as Faster R-CNN [32], SSD [33], and R-FCN [34]. These frameworks use a combination of CNNs and additional modules to generate candidate bounding boxes for objects in an image, which can then be classified and refined to produce the

final object detection output. One of the key advantages of these frameworks is that they can produce highly accurate object detections in a one-stage manner with no complex post-processing or refinement steps.

With the increasing prevalence of deep learning, a growing number of researchers in the field of medical imaging are currently focusing on integrating deep learning into their investigations [35]. For example, many recently proposed CAD systems for identifying pulmonary nodules utilize CNNs to achieve fast and accurate diagnoses. A survey discussed in [36] reveals that multiple CAD systems have emerged to detect nodules comprehensively. ZNET leverages CNNs for detecting candidates and reducing false positives. The input slices are cropped to dimensions of 512 × 512, and a U-Net model applies to each axial slice to create a probability map, which is utilized for identifying candidates. Subsequently, a threshold is used to obtain potential nodule regions, which is established with the objective of identifying the maximum possible number of nodules, based on the validation subset. Afterward, a 4-neighborhood kernel is applied for morphological erosion, which aids in eliminating the partial volume effects. A connected component analysis is utilized to group the candidates together, and the coordinates of the candidates are determined based on the centroid of the components. To decrease the occurrence of false positives, ZNET uses wide residual networks [37] and captures 64 * 64 image sections from the axial, sagittal, and coronal perspectives for each candidate, which are subsequently fed into the networks for independent processing. JianPeiCAD uses a rule-based screening at multiple scales to obtain potential nodules. To decrease false-positive results, a 3D CNN is employed with broad channels and is trained using data augmentation techniques. MOT_M5Lv1 [38] utilizes a technique called 3D region growing to obtain the lung volume, along with specific steps for excluding the trachea and separating the lungs. The algorithm for detecting candidates is derived from the approach presented by Messay et al. [39], which uses morphological processing and multiple gray-level thresholding to segment nodules. The elimination of false positives is carried out through the calculation of 15 features, which include geometrical and intensity features, and then classification is accomplished by utilizing feedforward neural networks. Resnet [40] suggests a framework for nodule detection using a 3D CNN. This framework screens candidates with a fully convolutional network and selects locations with high probabilities as candidates. To decrease the number of false positives, the recommendation is to incorporate multi-level contextual details surrounding pulmonary nodules by merging a collection of 3D CNNs with distinct receptive field sizes. This approach enables better differentiation of nodules from their challenging imitators. M5LCAD [41] uses ant colonies to segment the lung structures and performs a repetitive process of applying threshold values on the pheromone maps to obtain a set of possible candidates. To reduce the number of false positives, candidates are classified using a feedforward neural network based on a collection of 13 features, which encompass attributes related to spatial positioning, intensity values, and shape characteristics.

III. Proposed Method

A deep learning framework is being used for binary classification, as shown in Fig. 1. The CT image is taken as input and processed by three CNN feature extractors simultaneously. These extractors individually create a feature vector from the image, and the resulting vectors are merged and passed through fully connected layers, with the last being a Softmax layer that makes the final decision. Using an ensemble of extractors enables the model to generate multi-scale features, which enhance its capabilities and yield better outcomes than a single deep network.

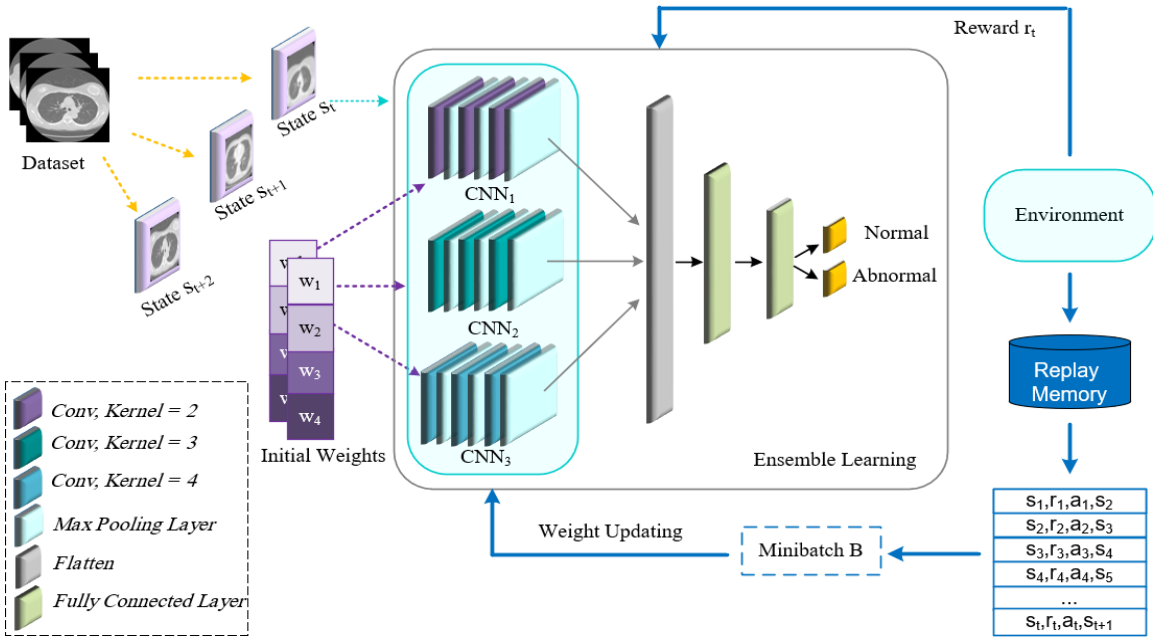

Fig. 1. The LLC-QE model.

The study utilized a CNN network architecture comprised of five convolution layers in two dimensions. The number of filters used in these layers was 128, 64, 32, 16, and 8. Each convolution layer has a kernel size of 2, stride of 3, and padding of 4 for both dimensions. The max-pooling layer has dimensions of 2 × 2, and there are three fully connected layers with hidden layer sizes of 128, 64, and 32. In order to avoid overfitting, early stopping and dropouts with a probability of 0.4 are utilized. The batch size for all experiments is 64, and the images in the dataset are gray scale, with light intensities mapped to the range [0,1].

A. Training

The training phase consists of two distinct and sequential steps: ABC pre-training is performed, and deep Q-network training is carried out. The ABC pre-trained weights are used to initialize the deep Q-network training.

1) ABC pre-training: The process helps established the network's initial values, increasing the probability of quicker convergence and reducing the chances of getting stuck in local optima. Initially, the weights of the CNN and feedforward layers are transformed into one unified vector, illustrated in Fig. 2. After that, the parameters of each convolutional layer and feedforward layer are compressed and combined into a single vector. Each potential solution for the flattened and concatenated vector is considered a food source in the ABC algorithm. The quality of a solution is evaluated by:

$$Fitness = \frac{1}{\sum_{i=1}^{N}(y_i - \tilde{y}_i)^2} \quad (1)$$

The formula evaluates the performance of the algorithm using N training images in the dataset. It considers the actual label y_i and the predicted label $\tilde{y}_i$ of the i-th data.

2) Deep Q-network training: Every CT image in the training set represents an environmental condition, while the system acts as the operative that performs a series of identifications across all CT pictures. When the operative determines the category tag of the CT picture, it is enacting a step: the picture observed at the t-th instance is the condition s_t, and the identification made is a_t. Consequently, the environment grants a benefit, r_t, to direct the operative. Reward figures are allocated in a manner where identifying an example from the dominant category earns a lesser absolute figure compared to the less common category. The reward function is:

$$r_t(s_t, a_t, y_t) = \begin{cases} +1, a_t = y_t \text{ and } s_t \in D_S \\ -1, a_t \neq y_t \text{ and } s_t \in D_S \\ \lambda, a_t = y_t \text{ and } s_t \in D_H \\ -\lambda, a_t \neq y_t \text{ and } s_t \in D_H \end{cases} \quad (2)$$

where D_S and D_H denote the less frequent and more prevalent classes, respectively. Properly or improperly categorizing an instance from the dominant class results in a reward of +λ or -λ, with $0 < \lambda < 1$.

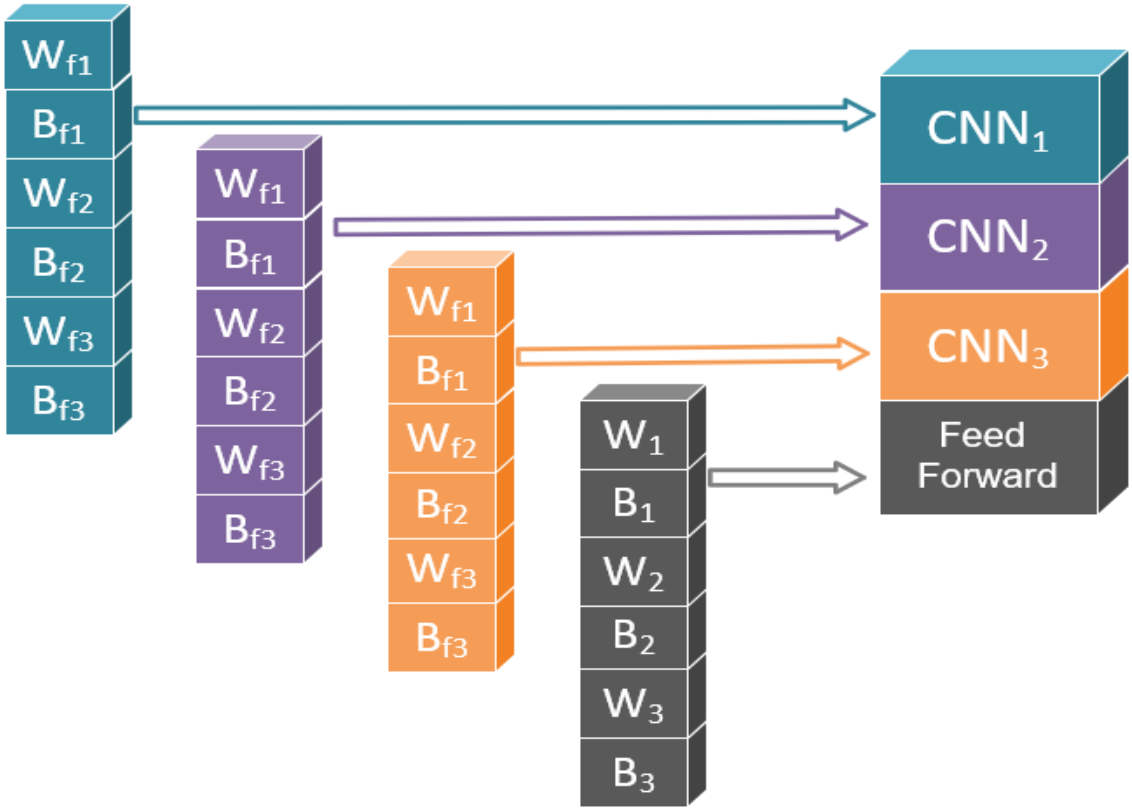

Fig. 2. The weights and biases of the neural network, starting from the initial convolutional layer up to the fully connected layers, are arranged and represented as individual elements in a large vector.

IV. Empirical Evaluation

A. Dataset

The Lung Image Database Consortium picture archive (LIDC-IDRI) [42] was established by the Foundation for the National Institutes of Health (FNIH) in collaboration with the Food and Drug Administration (FDA). This collection features a chest CT scan paired with an XML file, which records the annotations made by four radiologists, across 1,018 CT scans from 1,010 listed patients. The marking process comprises two phases aiming to pinpoint every nodule in the CT scans with the utmost precision. During the initial phase, termed the blinded-read phase, each radiologist individually reviewed the scans and identified lesions, noting them as "nodule <3 mm" or "non-nodule ≥3 mm". In the subsequent unblinded-read phase, each radiologist went over their annotations individually, while being conscious of the undisclosed annotations made by their peers. Within the collection, 7,371 lesions were identified as nodules by at least one radiologist. Out of these, 2,669 lesions were labeled as "nodule 3 mm" by at least one out of the four radiologists, with 928 being agreed upon by all. The 2,669 identified lesions were also provided with detailed nodule characteristics and defined outlines.

B. Experimental Results

Under prior experiments, k-fold cross-validation was employed throughout the study. In pursuit of this aim, the dataset is partitioned into k segments, assigning one for testing while employing the remaining for training. This process is reiterated k times, ensuring each datum is used once for testing and once for training. The resulting cross-validation statistical outcomes encompass metrics such as minimum, median, maximum mean, and standard deviation. However, mean values are used for comparative analysis.

The proposed approach is compared with ten state-of-the-art systems, including 3D-CNNs [43], ESB-ALL [44], Ali et al. [45], MGI-CNN [46], ODNN [47], Xie et al. [8], WOA_APSO [48], MEMCAP [4], LungNet-DL [49], and MetaCNN-LC [50]. In addition, comparing the proposed model with three primary methods unveils the impact of the ABC and RL components on the model's performance. The CNN + random weight method is a model that employs only the CNN network without the ABC algorithm and Reinforcement learning, while the CNN + ABC and CNN + RL models apply ABC and RL, respectively. The model performance on the LIDC dataset with the previously specified criteria is given in Table I and II. Achieving an Accuracy of 92.90%, a Recall of 92.00%, a Precision of 87.70%, an F-measure of 89.80%, a Specificity of 93.40%, and a G-means of 92.70%, the model shows notable distinctions from other deep models. LungNet-DL and MetaCNN-LC are the top two models after the algorithm, with 30% and 40% errors compared to LLC-QE + ABC, respectively. The proposed model reduces the error by over 60% compared with other deep algorithms. Comparing the LLC-QE + ABC model with the LLC + ABC and LLC + ABC models suggests that ABC and RL gimmicks have effectively reduced error by over 52% and 47%, respectively. The worst base model, LLC-QE + random weight, has been improved by approximately 67% by the proposed model.

TABLE I. The Results of Accuracy, Recall, and Precision for the Proposed Model and Other Algorithms

Method	Accuracy					Recall					Precision				
	min	***median***	***max***	***mean***	***std.dev.***	***min***	***median***	***max***	***mean***	***std.dev.***	***min***	***median***	***max***	***mean***	***std.dev.***
3D-CNNs [43]	0.752	0.789	0.830	0.793	0.029	0.673	0.748	0.804	0.751	0.052	0.621	0.669	0.723	0.672	0.037
ESB-ALL [44]	0.767	0.774	0.849	0.789	0.035	0.664	0.729	0.822	0.736	0.059	0.628	0.651	0.752	0.671	0.048
Ali et al. [45]	0.774	0.814	0.836	0.809	0.022	0.692	0.757	0.766	0.744	0.031	0.655	0.707	0.752	0.705	0.035
MGI-CNN [46]	0.789	0.814	0.858	0.819	0.026	0.738	0.776	0.86	0.787	0.048	0.669	0.711	0.754	0.709	0.033
ODNN [47]	0.789	0.821	0.862	0.821	0.027	0.729	0.766	0.879	0.781	0.058	0.672	0.718	0.752	0.714	0.029
Xie et al. [8]	0.792	0.821	0.871	0.825	0.032	0.748	0.794	0.822	0.785	0.029	0.672	0.719	0.817	0.723	0.059
WOA_APSO [48]	0.840	0.865	0.896	0.867	0.023	0.794	0.832	0.897	0.835	0.044	0.746	0.802	0.814	0.785	0.032
MEMCAP [4]	0.858	0.877	0.931	0.887	0.028	0.822	0.860	0.935	0.869	0.044	0.754	0.804	0.870	0.809	0.042
LungNet-DL [49]	0.871	0.886	0.930	0.892	0.036	0.842	0.862	0.923	0.869	0.012	0.776	0.816	0.876	0.824	0.123
MetaCNN-LC [50]	0.885	0.905	0.925	0.902	0.016	0.863	0.875	0.931	0.882	0.026	0.792	0.834	0.887	0.840	0.031
LLC-QE + random weight	0.755	0.792	0.805	0.783	0.023	0.766	0.813	0.841	0.809	0.03	0.603	0.654	0.669	0.641	0.029
LLC + ABC	0.818	0.849	0.881	0.849	0.023	0.785	0.850	0.897	0.843	0.044	0.706	0.744	0.78	0.743	0.026
LLC-QE	0.83	0.865	0.906	0.865	0.027	0.785	0.869	0.897	0.854	0.044	0.73	0.762	0.847	0.77	0.045
LLC-QE + ABC	0.915	0.931	0.943	0.929	0.011	0.888	0.916	0.944	0.920	0.022	0.860	0.883	0.894	0.877	0.015

TABLE II. THE RESULTS OF F-MEASURE, SPECIFICITY, AND G-MEANS FOR THE PROPOSED MODEL AND OTHER ALGORITHMS

Method	F-measure					Specificity					G-means				
	min	*median*	*max*	*mean*	*std.dev.*	*min*	*median*	*max*	*mean*	*std.dev.*	*min*	*median*	*max*	*mean*	*std.dev.*
3D-CNNs [43]	0.646	0.702	0.761	0.709	0.043	0.791	0.815	0.844	0.814	0.019	0.730	0.776	0.824	0.782	0.035
ESB-ALL [44]	0.657	0.686	0.785	0.701	0.049	0.773	0.820	0.863	0.816	0.032	0.738	0.765	0.842	0.775	0.040
Ali et al. [45]	0.673	0.733	0.759	0.724	0.032	0.815	0.839	0.872	0.842	0.020	0.751	0.799	0.817	0.791	0.025
MGI-CNN [46]	0.702	0.733	0.804	0.746	0.039	0.815	0.844	0.858	0.836	0.018	0.776	0.799	0.859	0.811	0.032
ODNN [47]	0.699	0.742	0.811	0.746	0.041	0.820	0.844	0.853	0.842	0.013	0.773	0.806	0.866	0.811	0.034
Xie et al. [8]	0.708	0.742	0.805	0.752	0.038	0.806	0.848	0.910	0.845	0.041	0.781	0.806	0.850	0.814	0.028
WOA_APSO [48]	0.769	0.798	0.853	0.809	0.034	0.863	0.896	0.900	0.884	0.019	0.828	0.847	0.896	0.859	0.028
MEMCAP [4]	0.804	0.822	0.901	0.838	0.040	0.858	0.896	0.929	0.896	0.025	0.858	0.868	0.932	0.882	0.031
LungNet-DL [49]	0.825	0.841	0.894	0.864	0.022	0.862	0.905	0.923	0.913	0.035	0.862	0.885	0.905	0.892	0.014
MetaCNN-LC [50]	0.842	0.863	0.906	0.896	0.026	0.876	0.914	0.935	0.926	0.032	0.872	0.896	0.914	0.906	0.009
LLC-QE + random weight	0.683	0.725	0.742	0.715	0.029	0.735	0.782	0.791	0.770	0.023	0.762	0.797	0.811	0.789	0.024
LLC + ABC	0.743	0.791	0.834	0.789	0.033	0.834	0.848	0.872	0.852	0.014	0.809	0.849	0.884	0.847	0.028
LLC-QE	0.757	0.812	0.863	0.810	0.038	0.848	0.863	0.919	0.870	0.028	0.818	0.866	0.899	0.862	0.030
LLC-QE + ABC	0.876	0.899	0.918	0.898	0.017	0.924	0.938	0.943	0.934	0.008	0.908	0.927	0.943	0.927	0.014

The aim is to carry out an additional experiment to assess the influence of employing distinct algorithms for initializing the model parameters. To achieve this aim, in order to maintain a fair assessment, all components of the model will remain unchanged–encompassing reinforcement learning and the CNN structure–with alterations limited solely to the initialization algorithm. Substitution of the algorithmic instructor will involve five established conventional algorithms, including GDM [51], GDA [52], GDMA [53], OSS [54], and BR [55], and four metaheuristic algorithms, including GWO [56], BA [57], COA [58] and WOA [59]. The ABC algorithm used in the model outperforms all other meta-heuristic algorithms (Table III and IV).

TABLE III. THE RESULTS OF ACCURACY, RECALL, AND PRECISION FOR THE CONVENTIONAL AND METAHEURISTIC ALGORITHMS

Method	Accuracy					Recall					Precision				
	min	***median***	***max***	***mean***	***std.dev.***	***min***	***median***	***max***	***mean***	***std.dev.***	***min***	***median***	***max***	***mean***	***std.dev.***
LLC-QE + GDM	0.805	0.865	0.906	0.864	0.039	0.748	0.794	0.888	0.806	0.059	0.696	0.802	0.841	0.793	0.058
LLC-QE + GDA	0.824	0.881	0.899	0.872	0.029	0.785	0.841	0.879	0.841	0.035	0.718	0.800	0.832	0.793	0.046
LLC-QE + GDMA	0.827	0.849	0.865	0.848	0.014	0.776	0.785	0.841	0.798	0.028	0.728	0.764	0.79	0.763	0.023
LLC-QE + OSS	0.849	0.871	0.884	0.867	0.015	0.748	0.813	0.869	0.806	0.056	0.788	0.806	0.813	0.801	0.011
LLC-QE + BR	0.843	0.862	0.884	0.863	0.016	0.757	0.804	0.869	0.806	0.050	0.771	0.789	0.802	0.791	0.013
LLC-QE + GWO	0.858	0.865	0.896	0.869	0.016	0.776	0.813	0.841	0.807	0.027	0.786	0.798	0.849	0.805	0.025
LLC-QE + BAT	0.852	0.868	0.877	0.865	0.010	0.766	0.785	0.832	0.794	0.031	0.778	0.804	0.828	0.804	0.019
LLC-QE + COA	0.821	0.877	0.881	0.864	0.025	0.738	0.832	0.841	0.811	0.044	0.731	0.804	0.811	0.79	0.034
LLC-QE + WOA	0.833	0.881	0.899	0.874	0.026	0.841	0.841	0.879	0.852	0.017	0.714	0.811	0.832	0.792	0.049

TABLE IV. THE RESULTS OF F-MEASURE, SPECIFICITY, AND G-MEANS FOR THE CONVENTIONAL AND METAHEURISTIC ALGORITHMS

Method	F-measure					Specificity					G-means				
	min	*median*	*max*	*mean*	*std.dev.*	*min*	*median*	*max*	*mean*	*std.dev.*	*min*	*median*	*max*	*mean*	*std.dev.*
LLC-QE + GDM	0.721	0.798	0.864	0.799	0.056	0.834	0.900	0.915	0.893	0.034	0.79	0.845	0.901	0.848	0.043
LLC-QE + GDA	0.750	0.829	0.855	0.816	0.040	0.844	0.891	0.910	0.888	0.027	0.814	0.875	0.894	0.864	0.03
LLC-QE + GDMA	0.751	0.783	0.807	0.780	0.020	0.853	0.877	0.896	0.874	0.016	0.814	0.834	0.859	0.835	0.016
LLC-QE + OSS	0.769	0.809	0.831	0.803	0.028	0.882	0.900	0.910	0.898	0.010	0.82	0.855	0.875	0.85	0.026
LLC-QE + BR	0.764	0.796	0.834	0.797	0.028	0.886	0.891	0.905	0.892	0.008	0.819	0.846	0.88	0.847	0.025
LLC-QE + GWO	0.787	0.804	0.845	0.806	0.024	0.886	0.896	0.924	0.900	0.014	0.836	0.853	0.882	0.853	0.018
LLC-QE + BAT	0.781	0.796	0.818	0.799	0.016	0.886	0.905	0.919	0.901	0.013	0.833	0.839	0.863	0.846	0.015
LLC-QE + COA	0.734	0.820	0.826	0.800	0.038	0.863	0.896	0.900	0.891	0.016	0.798	0.865	0.87	0.85	0.03
LLC-QE + WOA	0.772	0.826	0.855	0.821	0.033	0.829	0.900	0.910	0.885	0.034	0.835	0.87	0.894	0.869	0.023

1) Impact of the reward function: The rewards for accurate and erroneous categorizations are given to the predominant and less frequent classes as ±1 and ±λ, respectively. The λ value is influenced by the ratio of dominant to fewer common examples, and it is expected that as this ratio rises, the ideal λ value will drop. To explore the influence of λ, we evaluated the suggested model's effectiveness across various λ values, which spanned from 0 to 1, at 0.1 intervals, while keeping the rewards for the dominant class unaltered. These outcomes are depicted in Fig. 3. When λ is zero, the dominant class's influence is minimal, and at λ = 1, both classes have equivalent influences. Fig. 3 reveals that the model's optimal performance is achieved when λ is 0.4, across all evaluated metrics. This suggests that the best λ value is neither zero nor one, but falls somewhere between these extremes. It is crucial to highlight that, while it is essential to reduce the dominant class's influence by tweaking λ, setting it excessively low might degrade the model's overall effectiveness. The findings indicate that selecting an appropriate λ value profoundly affects the LLC-QE model's efficiency. The best λ value is influenced by the respective quantities of dominant and less frequent examples, making it crucial to determine it prudently for optimal outcomes.

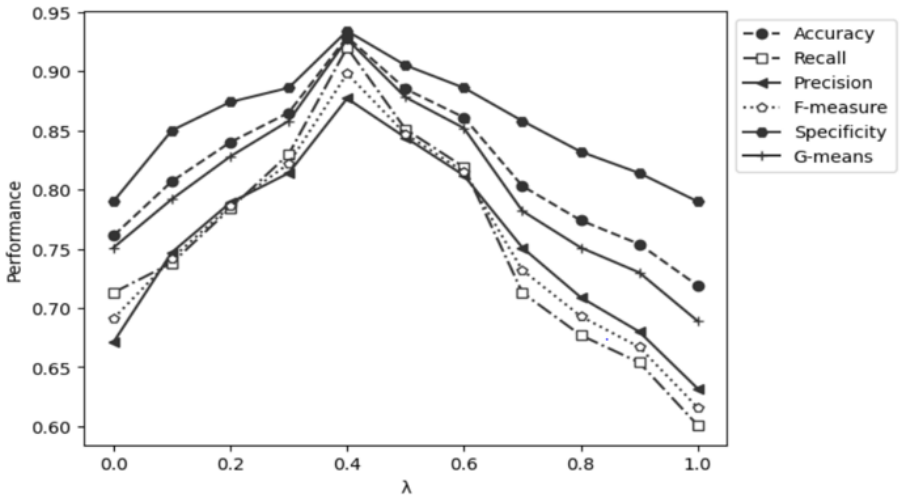

Fig. 3. LLC-QE model performance metrics plotted against the value of λ in the reward function.

2) Impact of the number of CNNs: The LLC-QE model uses a group of CNNs to derive feature vectors from input images simultaneously. The number of CNN feature extractors can significantly impact the model's overall performance. Using too few CNNs could cause insufficient feature extraction, while using too many CNNs could lead to overfitting or redundant information extraction, both of which may negatively impact the model's performance. The performance of the LLC-QE model was assessed by altering the count of CNN feature extractors across the range of one to seven. This variation is aimed at identifying the optimal number of extractors. The findings indicated optimal performance was achieved when three CNNs were used, as shown in Fig. 4. The model's performance decreased as the number of CNNs increased, with performing six and seven CNNs being worse than that of a single CNN. The optimal number of CNNs was determined based on performance metrics.

3) Impact of the loss function: Classification problems caused by imbalanced datasets can also address using conventional methods, such as altering the loss function and using data augmentation. However, their effectiveness depends highly on the specific problem being addressed. Meanwhile, the loss function plays a more significant role, as it can give more prominence to the minority class. To study the inefficiency of the loss functions on the training ANN, the selection encompassed five functions, including Weighted Cross-Entropy (WCE) [60], Balanced Cross-Entropy (BCE) [61], Dice Loss (DL) [62], Tversky Loss (TL) [63], and Focal Loss (FL) [64]. WCE and BCE both assign weights to positive and negative samples. FL, suited for imbalanced data, outperforms the other loss function (Table V) but is still inferior to the RL used in the model.

4) Impact of pre-trained models: Comparing the performance of the CNN ensemble model with that of alternative pre-trained feature extraction models involved replacing the model with transfer learning counterparts, such as AlexNet [65], GoogleNet [66], ResNet [67], DenseNet [68], and MobileNet [69]. Limiting the training solely to the feedforward network, superior performance is exhibited by the model's ensemble of CNNs. This ensemble, trained from the ground up, surpasses the performance of pre-trained networks (AlexNet, GoogleNet, ResNet, DenseNet, and MobileNet), as demonstrated in Table VI. The reason behind this is that the ensemble of CNNs is more capable of extracting discriminative features specific to cancer diagnosis.

TABLE V. PERFORMANCE OF THE PROPOSED MODEL FOR DIFFERENT LOSS FUNCTIONS

Method	Accuracy	Sensitivity	Precision	F-measure	Specificity	G-mean
WCE	0.830	0.885	0.790	0.803	0.778	0.845
BCE	0.822	0.821	0.783	0.745	0.824	0.822
DL	0.816	0.795	0.769	0.711	0.837	0.811
TL	0.825	0.834	0.78	0.747	0.816	0.827
FL	0.861	0.889	0.826	0.819	0.833	0.868

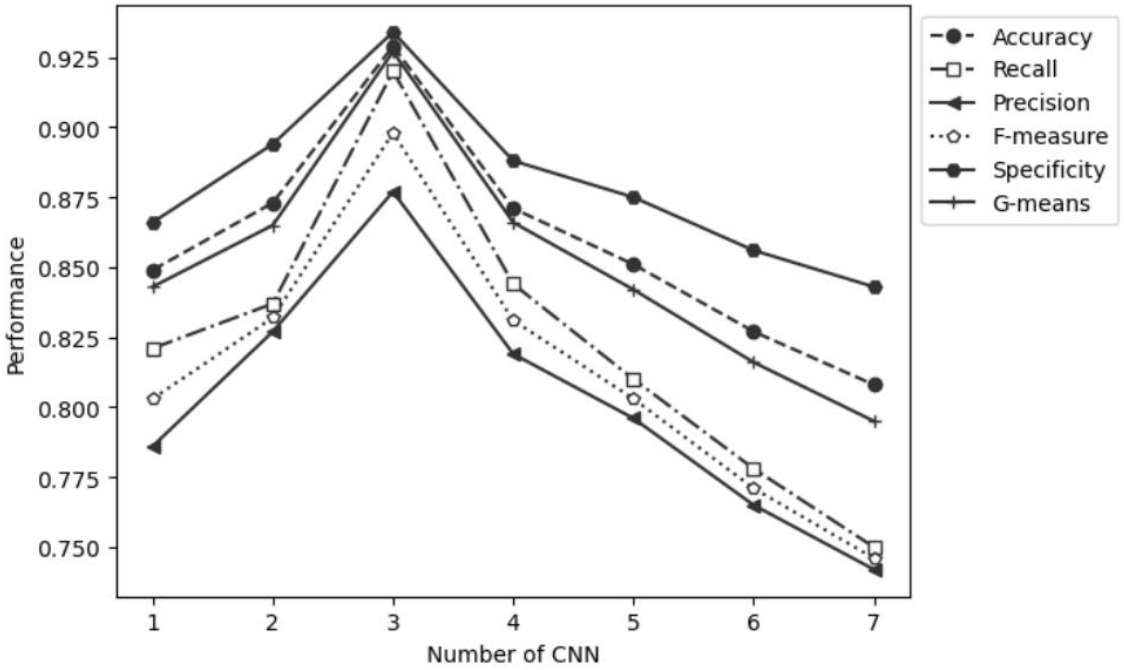

Fig. 4. The performance metrics plotted vs the number of convolutional feature extractors working in the ensemble.

TABLE VI. PERFORMANCE OF THE PROPOSED MODEL FOR DIFFERENT PRE-TRAINED MODELS

Method	Accuracy	Sensitivity	Precision	F-measure	Specificity	G-mean
AlexNet	0.773	0.836	0.719	0.724	0.715	0.790
GoogleNet	0.789	0.768	0.737	0.676	0.811	0.784
ResNet	0.764	0.794	0.709	0.683	0.736	0.772
DenseNet	0.753	0.759	0.696	0.651	0.748	0.755
MobileNet	0.784	0.806	0.731	0.703	0.762	0.789

V. CONCLUSION

This article proposes a novel deep-learning approach that uses RL and evolutionary computation to classify lung cancer in CT images. To avoid the model getting trapped in local optima, the network weights are first initialized using the evolutionary ABC algorithm. The network architecture comprises an ensemble of CNNs that extract features in parallel and then concatenate them for downstream classification. The model uses RL to address the dataset imbalance. The proposed LLC-QE model achieves excellent results compared to other deep learning models and pre-trained transfer learning models when trained on the LIDC-IDRI dataset. The optimal value for the reward function and the optimal number of CNN feature extractors in the ensemble are determined through experiments on the study dataset. Separate ablation studies, excluding ABC pre-training and RL, confirm the positive incremental impact of these components on model performance. Notably, the ABC algorithm and RL outperform various meta-heuristic initialization algorithms and loss functions.

Future work aims to develop deep learning segmentation methods that can detect not only the presence of cancer but also the location and extent of the disease on CT images, which may be useful for prognostication and therapeutic monitoring. One area of research that holds particular promise is the use of multi-modal imaging data, which can provide a more comprehensive view of the tumor and its surroundings. For example, combining CT with MRI data could allow for more accurate identification of the tumor boundary and help differentiate between different cancers.

FUNDING

This work was supported by Science and Technology Research Project of Jiangxi Provincial Department of Education (GJJ2202030), and Natural Science Research Project of Nanchang Normal University (22XJZR02).

REFERENCES

[1] S. Danaei et al., "Myocarditis Diagnosis: A Method using Mutual Learning-Based ABC and Reinforcement Learning," in 2022 IEEE 22nd International Symposium on Computational Intelligence and Informatics and 8th IEEE International Conference on Recent Achievements in Mechatronics, Automation, Computer Science and Robotics (CINTI-MACRo), 2022: IEEE, pp. 000265-000270.

[2] R. L. Siegel, K. D. Miller, and A. Jemal, "Cancer statistics, 2016," CA: a cancer journal for clinicians, vol. 66, no. 1, pp. 7-30, 2016.

[3] H. Zareiamand, A. Darroudi, I. Mohammadi, S. V. Moravvej, S. Danaei, and R. Alizadehsani, "Cardiac Magnetic Resonance Imaging (CMRI) Applications in Patients with Chest Pain in the Emergency Department: A Narrative Review," Diagnostics, vol. 13, no. 16, p. 2667, 2023.

[4] A. Mobiny et al., "Memory-augmented capsule network for adaptable lung nodule classification," IEEE Transactions on Medical Imaging, 2021.

[5] L. Hong et al., "GAN-LSTM-3D: An efficient method for lung tumour 3D reconstruction enhanced by attention-based LSTM," CAAI Transactions on Intelligence Technology, 2023.

[6] S. V. Moravvej et al., "RLMD-PA: A reinforcement learning-based myocarditis diagnosis combined with a population-based algorithm for pretraining weights," Contrast Media & Molecular Imaging, vol. 2022, 2022.

[7] I. Sluimer, A. Schilham, M. Prokop, and B. Van Ginneken, "Computer analysis of computed tomography scans of the lung: a survey," IEEE transactions on medical imaging, vol. 25, no. 4, pp. 385-405, 2006.

[8] H. Xie, D. Yang, N. Sun, Z. Chen, and Y. Zhang, "Automated pulmonary nodule detection in CT images using deep convolutional neural networks," Pattern Recognition, vol. 85, pp. 109-119, 2019.

[9] J. Ning, H. Zhao, L. Lan, P. Sun, and Y. Feng, "A computer-aided detection system for the detection of lung nodules based on 3D-ResNet," Applied Sciences, vol. 9, no. 24, p. 5544, 2019.

[10] M. A. Wiering, H. Van Hasselt, A.-D. Pietersma, and L. Schomaker, "Reinforcement learning algorithms for solving classification problems," 2011: IEEE, pp. 91-96.

[11] N. Tajbakhsh and K. Suzuki, "Comparing two classes of end-to-end machine-learning models in lung nodule detection and classification: MTANNs vs. CNNs," Pattern recognition, vol. 63, pp. 476-486, 2017.

[12] S. V. Moravvej, S. J. Mousavirad, D. Oliva, and F. Mohammadi, "A Novel Plagiarism Detection Approach Combining BERT-based Word Embedding, Attention-based LSTMs and an Improved Differential Evolution Algorithm," arXiv preprint arXiv:2305.02374, 2023.

[13] H. Han, W.-Y. Wang, and B.-H. Mao, "Borderline-SMOTE: a new over-sampling method in imbalanced data sets learning," in International conference on intelligent computing, 2005: Springer, pp. 878-887.

[14] I. Mani and I. Zhang, "kNN approach to unbalanced data distributions: a case study involving information extraction," in Proceedings of workshop on learning from imbalanced datasets, 2003, vol. 126: ICML United States.

[15] S. V. Moravvej, S. J. Mousavirad, M. H. Moghadam, and M. Saadatmand, "An LSTM-based plagiarism detection via attention mechanism and a population-based approach for pre-training parameters with imbalanced classes," in Neural Information Processing: 28th International Conference, ICONIP 2021, Sanur, Bali, Indonesia, December 8–12, 2021, Proceedings, Part III 28, 2021: Springer, pp. 690-701.

[16] K. Arulkumaran, M. P. Deisenroth, M. Brundage, and A. A. Bharath, "Deep reinforcement learning: A brief survey," IEEE Signal Processing Magazine, vol. 34, no. 6, pp. 26-38, 2017.

[17] M. A. Wiering, H. Van Hasselt, A.-D. Pietersma, and L. Schomaker, "Reinforcement learning algorithms for solving classification problems," in 2011 IEEE Symposium on Adaptive Dynamic Programming and Reinforcement Learning (ADPRL), 2011: IEEE, pp. 91-96.

[18] T. Zhang, M. Huang, and L. Zhao, "Learning structured representation for text classification via reinforcement learning," in Thirty-Second AAAI Conference on Artificial Intelligence, 2018.

[19] D. Liu and T. Jiang, "Deep reinforcement learning for surgical gesture segmentation and classification," in International conference on medical image computing and computer-assisted intervention, 2018: Springer, pp. 247-255.

[20] D. Zhao, Y. Chen, and L. Lv, "Deep reinforcement learning with visual attention for vehicle classification," IEEE Transactions on Cognitive and Developmental Systems, vol. 9, no. 4, pp. 356-367, 2016.

[21] J. Janisch, T. Pevný, and V. Lisý, "Classification with costly features using deep reinforcement learning," in Proceedings of the AAAI

Conference on Artificial Intelligence, 2019, vol. 33, no. 01, pp. 3959-3966.

[22] L. Abdi and S. Hashemi, "An ensemble pruning approach based on reinforcement learning in presence of multi-class imbalanced data," in Proceedings of the Third International Conference on Soft Computing for Problem Solving, 2014: Springer, pp. 589-600.

[23] S. Vakilian, S. V. Moravvej, and A. Fanian, "Using the artificial bee colony (ABC) algorithm in collaboration with the fog nodes in the Internet of Things three-layer architecture," in 2021 29th Iranian Conference on Electrical Engineering (ICEE), 2021: IEEE, pp. 509-513.

[24] S. Vakilian, S. V. Moravvej, and A. Fanian, "Using the cuckoo algorithm to optimizing the response time and energy consumption cost of fog nodes by considering collaboration in the fog layer," in 2021 5th International Conference on Internet of Things and Applications (IoT), 2021: IEEE, pp. 1-5.

[25] S. V. Moravvej, S. J. Mousavirad, D. Oliva, G. Schaefer, and Z. Sobhaninia, "An improved de algorithm to optimise the learning process of a bert-based plagiarism detection model," in 2022 IEEE Congress on Evolutionary Computation (CEC), 2022: IEEE, pp. 1-7.

[26] K.-L. Hua, C.-H. Hsu, S. C. Hidayati, W.-H. Cheng, and Y.-J. Chen, "Computer-aided classification of lung nodules on computed tomography images via deep learning technique," OncoTargets and therapy, pp. 2015-2022, 2015.

[27] H. Xie, Y. Zhang, K. Gao, S. Tang, K. Xu, L. Guo, and J. Li, "Robust common visual pattern discovery using graph matching," Journal of visual communication and image representation, vol. 24, no. 5, pp. 635-646, 2013.

[28] M. Tan, R. Deklerck, B. Jansen, M. Bister, and J. Cornelis, "A novel computer-aided lung nodule detection system for CT images," Medical physics, vol. 38, no. 10, pp. 5630-5645, 2011.

[29] A. Traverso, E. L. Torres, M. Fantacci, and P. Cerello, "Computer-aided detection systems to improve lung cancer early diagnosis: state-of-the-art and challenges," in Journal of Physics: Conference Series, 2017, vol. 841, no. 1: IOP Publishing, p. 012013.

[30] T. Liu, W. Xu, P. Spincemaille, A. S. Avestimehr, and Y. Wang, "Accuracy of the morphology enabled dipole inversion (MEDI) algorithm for quantitative susceptibility mapping in MRI," IEEE transactions on medical imaging, vol. 31, no. 3, pp. 816-824, 2012.

[31] H. Xie, K. Gao, Y. Zhang, and J. Li, "Local geometric consistency constraint for image retrieval," in 2011 18th IEEE International Conference on Image Processing, 2011: IEEE, pp. 101-104.

[32] S. Ren, K. He, R. Girshick, and J. Sun, "Faster r-cnn: Towards real-time object detection with region proposal networks," Advances in neural information processing systems, vol. 28, 2015.

[33] W. Liu, D. Anguelov, D. Erhan, C. Szegedy, S. Reed, C.-Y. Fu, and A. C. Berg, "Ssd: Single shot multibox detector," in Computer Vision–ECCV 2016: 14th European Conference, Amsterdam, The Netherlands, October 11–14, 2016, Proceedings, Part I 14, 2016: Springer, pp. 21-37.

[34] J. Dai, Y. Li, K. He, and J. Sun, "R-fcn: Object detection via region-based fully convolutional networks," Advances in neural information processing systems, vol. 29, 2016.

[35] K.-L. Hua, H.-C. Wang, C.-H. Yeh, W.-H. Cheng, and Y.-C. Lai, "Background extraction using random walk image fusion," IEEE transactions on cybernetics, vol. 48, no. 1, pp. 423-435, 2016.

[36] A. A. A. Setio et al., "Validation, comparison, and combination of algorithms for automatic detection of pulmonary nodules in computed tomography images: the LUNA16 challenge," Medical image analysis, vol. 42, pp. 1-13, 2017.

[37] S. Zagoruyko and N. Komodakis, "Wide residual networks," arXiv preprint arXiv:1605.07146, 2016.

[38] Q. Dou, H. Chen, Y. Jin, H. Lin, J. Qin, and P.-A. Heng, "Automated pulmonary nodule detection via 3d convnets with online sample filtering and hybrid-loss residual learning," in Medical Image Computing and Computer Assisted Intervention− MICCAI 2017: 20th International Conference, Quebec City, QC, Canada, September 11-13, 2017, Proceedings, Part III 20, 2017: Springer, pp. 630-638.

[39] T. Messay, R. C. Hardie, and S. K. Rogers, "A new computationally efficient CAD system for pulmonary nodule detection in CT imagery," Medical image analysis, vol. 14, no. 3, pp. 390-406, 2010.

[40] Q. Dou, H. Chen, L. Yu, J. Qin, and P.-A. Heng, "Multilevel contextual 3-D CNNs for false positive reduction in pulmonary nodule detection," IEEE Transactions on Biomedical Engineering, vol. 64, no. 7, pp. 1558-1567, 2016.

[41] E. Lopez Torres et al., "Large scale validation of the M5L lung CAD on heterogeneous CT datasets," Medical physics, vol. 42, no. 4, pp. 1477-1489, 2015.

[42] L. M. Pehrson, M. B. Nielsen, and C. Ammitzbøl Lauridsen, "Automatic pulmonary nodule detection applying deep learning or machine learning algorithms to the LIDC-IDRI database: a systematic review," Diagnostics, vol. 9, no. 1, p. 29, 2019.

[43] P. Monkam, S. Qi, M. Xu, H. Li, F. Han, Y. Teng, and W. Qian, "Ensemble learning of multiple-view 3D-CNNs model for micro-nodules identification in CT images," IEEE Access, vol. 7, pp. 5564-5576, 2018.

[44] H. Jung, B. Kim, I. Lee, J. Lee, and J. Kang, "Classification of lung nodules in CT scans using three-dimensional deep convolutional neural networks with a checkpoint ensemble method," BMC medical imaging, vol. 18, no. 1, pp. 1-10, 2018.

[45] I. Ali et al., "Lung nodule detection via deep reinforcement learning," Frontiers in oncology, vol. 8, p. 108, 2018.

[46] B.-C. Kim, J. S. Yoon, J.-S. Choi, and H.-I. Suk, "Multi-scale gradual integration CNN for false positive reduction in pulmonary nodule detection," Neural Networks, vol. 115, pp. 1-10, 2019.

[47] S. Lakshmanaprabu, S. N. Mohanty, K. Shankar, N. Arunkumar, and G. Ramirez, "Optimal deep learning model for classification of lung cancer on CT images," Future Generation Computer Systems, vol. 92, pp. 374-382, 2019.

[48] S. Vijh, P. Gaurav, and H. M. Pandey, "Hybrid bio-inspired algorithm and convolutional neural network for automatic lung tumor detection," Neural Computing and Applications, pp. 1-14, 2020.

[49] R. Tandon, S. Agrawal, R. Raghuwanshi, N. P. S. Rathore, L. Prasad, and V. Jain, "Automatic lung carcinoma identification and classification in CT images using CNN deep learning model," in Augmented Intelligence in Healthcare: A Pragmatic and Integrated Analysis: Springer, 2022, pp. 143-166.

[50] T. I. Mohamed, O. N. Oyelade, and A. E. Ezugwu, "Automatic detection and classification of lung cancer CT scans based on deep learning and ebola optimization search algorithm," PloS one, vol. 18, no. 8, p. e0285796, 2023.

[51] V. Phansalkar and P. Sastry, "Analysis of the back-propagation algorithm with momentum," IEEE Transactions on Neural Networks, vol. 5, no. 3, pp. 505-506, 1994.

[52] M. Hagan, H. Demuth, and M. Beale, "Neural Network Design (PWS, Boston, MA)," Google Scholar Google Scholar Digital Library Digital Library, 1996.

[53] C.-C. Yu and B.-D. Liu, "A backpropagation algorithm with adaptive learning rate and momentum coefficient," in Proceedings of the 2002 International Joint Conference on Neural Networks. IJCNN'02 (Cat. No. 02CH37290), 2002, vol. 2: IEEE, pp. 1218-1223.

[54] R. Battiti, "First-and second-order methods for learning: between steepest descent and Newton's method," Neural computation, vol. 4, no. 2, pp. 141-166, 1992.

[55] F. D. Foresee and M. T. Hagan, "Gauss-Newton approximation to Bayesian learning," in Proceedings of international conference on neural networks (ICNN'97), 1997, vol. 3: IEEE, pp. 1930-1935.

[56] S. Mirjalili, S. M. Mirjalili, and A. Lewis, "Grey wolf optimizer," Advances in engineering software, vol. 69, pp. 46-61, 2014.

[57] X.-S. Yang, "A new metaheuristic bat-inspired algorithm," in Nature inspired cooperative strategies for optimization (NICSO 2010): Springer, 2010, pp. 65-74.

[58] X.-S. Yang and S. Deb, "Cuckoo search via Lévy flights," in 2009 World congress on nature & biologically inspired computing (NaBIC), 2009: Ieee, pp. 210-214.

[59] S. Mirjalili and A. Lewis, "The whale optimization algorithm," Advances in engineering software, vol. 95, pp. 51-67, 2016.

[60] V. Pihur, S. Datta, and S. Datta, "Weighted rank aggregation of cluster validation measures: a monte carlo cross-entropy approach," Bioinformatics, vol. 23, no. 13, pp. 1607-1615, 2007.

[61] S. Xie and Z. Tu, "Holistically-nested edge detection," in Proceedings of the IEEE international conference on computer vision, 2015, pp. 1395-1403.

[62] C. H. Sudre, W. Li, T. Vercauteren, S. Ourselin, and M. J. Cardoso, "Generalised dice overlap as a deep learning loss function for highly unbalanced segmentations," in Deep learning in medical image analysis and multimodal learning for clinical decision support: Springer, 2017, pp. 240-248.

[63] S. S. M. Salehi, D. Erdogmus, and A. Gholipour, "Tversky loss function for image segmentation using 3D fully convolutional deep networks," in International workshop on machine learning in medical imaging, 2017: Springer, pp. 379-387.

[64] T.-Y. Lin, P. Goyal, R. Girshick, K. He, and P. Dollár, "Focal loss for dense object detection," in Proceedings of the IEEE international conference on computer vision, 2017, pp. 2980-2988.

[65] M. Z. Alom et al., "The history began from alexnet: A comprehensive survey on deep learning approaches," arXiv preprint arXiv:1803.01164, 2018.

[66] R. Anand, T. Shanthi, M. Nithish, and S. Lakshman, "Face recognition and classification using GoogleNET architecture," in Soft Computing for Problem Solving: SocProS 2018, Volume 1, 2020: Springer, pp. 261-269.

[67] S. Targ, D. Almeida, and K. Lyman, "Resnet in resnet: Generalizing residual architectures," arXiv preprint arXiv:1603.08029, 2016.

[68] G. Huang, Z. Liu, L. Van Der Maaten, and K. Q. Weinberger, "Densely connected convolutional networks," in Proceedings of the IEEE conference on computer vision and pattern recognition, 2017, pp. 4700-4708.

[69] A. G. Howard et al., "Mobilenets: Efficient convolutional neural networks for mobile vision applications," arXiv preprint arXiv:1704.04861, 2017.